Supporting information

Ultra-high-rate CO_2 reduction reactions to multicarbon products with a current density of 1.7 A/cm^2 in neutral electrolyte

Asato Inoue[a], *Takashi Harada*[a], *Shuji Nakanishi** [a,b], *Kazuhide Kamiya** [a,b]

[a] Research Center for Solar Energy Chemistry, Graduate School of Science Engineering, Osaka University, 1-3 Machikaneyama, Toyonaka, Osaka 560-8531, Japan.

[b] Innovative Catalysis Science Division, Institute for Open and Transdisciplinary Research Initiatives (ICS-OTRI), Osaka University, Suita, Osaka 565-0871, Japan.

Corresponding authors: nakanishi.shuji.es@osaka-u.ac.jp (S.N.), kamiya.kazuhide.es@osaka-u.ac.jp (K.K.)

Experimental Section

Chemical and materials

$Cu(CH_3COO)_2 \cdot H_2O$ (99.99% trace metals basis) and 5 wt% Nafion dispersion were obtained from Sigma-Aldrich Chemical Co., Ltd. $NaBH_4$, ethanol, isopropanol, DMSO, KCl, KOH and $KHCO_3$ were purchased from Wako Co., Ltd. We prepared three kinds of commercial carbon-based gas diffusion electrodes, GDL 34BC (Sigracet), GDS2130 (AvCarb) and PYROFIL MFK-A (Mitsubishi Chemical Co., Ltd.). Cu-based catalysts, in addition to the synthesized one as below, were purchased from Sigma-Aldrich Chemical Co., Ltd. A PTFE to be pasted to fix an electrode area was NITOFLON^{TM} (No.900UL, thickness: 0.2 mm, Nitto). A proton-exchange membrane (Nafion 117) was purchased from Fuel Cell Store.

Preparation of the electrodes

We here explain how to prepare our optimized electrode. CuONPs were synthesized via a wet-chemical reduction method. Briefly, 0.61 g of $Cu(CH_3COO)_2 \cdot H_2O$ was dissolved in 250 mL of deionized water, and the resultant solution was stirred under Ar bubbling for 30 min to remove residual oxygen. 1.25 g of $NaBH_4$ in 20 mL of deionized water was dropped slowly into the copper(II) ion solutions. The synthesized metal Cu nanoparticles were rinsed with deionized water and ethanol. Then, we stored them at room temperature under ambient conditions for at least two weeks to oxidize by air. A homogeneous catalyst ink was prepared by sonication of 3.4 mg of CuONPs with 400 μL of isopropanol and 4.4 μL of a 5 wt% Nafion dispersion. The catalyst ink was drop-casted onto a GDL34BC at 80 °C. A PTFE sheet with a hole (0.5 cm^2) was pasted on the GDE by hot pressing (250 °C, 10 MPa for 1 minute) before catalyst coating to strictly fix the area of the electrode. The pasted PTFE would also be beneficial to suppress HER from the bare MPL. The target amount of CuONPs loading was obtained by repeatedly loading and drying the catalyst ink of 20 μl. We prepared electrodes with the same method even when varying catalysts or GDEs.

Characterization

Transmission electron microscopy (TEM) observation were conducted using a Hitachi H-9000NAR microscope. X-ray diffraction (XRD patterns) were collected using a Miniflex diffractmeter (Rigaku) equipped with a Cu Kα radiation source. X-ray photoelectron spectroscopy (XPS) analyses were conducted using an Axis Ultra spectrometer (Kratos Analytical) equipped with an Al Kα radiation source. Field-emission scanning electron microscopy (FESEM) images were obtained using a JEOL JSM-7800F microscope.

Energy dispersive X-ray spectroscopy (EDX) elemental mappings were acquired using an Oxford Instruments X-MaxN spectrometer.

Electrochemical experiments

Electrochemical experiments were performed using electrochemical workstations (HAL3001A+HAL3001B10, Hokuto Denko and SI1287, Solartron). An in-house-built three-compartment electrochemical cell was used for all experiments (Figure S12). A proton-exchange membrane (Nafion 117) was used to separate the cathodic and anodic chambers. A Pt wire and an Ag/AgCl electrode with 3 M KCl solution were used as counter and reference electrodes, respectively. During the electrochemical experiments, CO_2 gas (99.99%) was supplied into the gas chamber at a rate of 15 sccm. Both catholyte and anolyte were flowed at a rate of 10 mL/min using peristaltic pumps and passed once through each chamber without circulation. The temperature of the catholyte at the outlet was 40 °C and constant during electrolysis. We used 1 M KOH and saturated $KHCO_3$ solutions as anolyte for alkaline and neutral CO_2RR, respectively. Saturated $KHCO_3$ solution was used for anolyte to reduce cell voltage. The gaseous products were analyzed using gas chromatography (GC-2030, Shimadzu) equipped with both thermal conductivity detector (TCD) and flame ionization detector (FID) as detectors, and

MICROPACKED-ST (Shinwa Chemical Industries Ltd.) as columns. The liquid products were analyzed using NMR spectroscopy (Unity-Inova500, Agilent) using presaturation mode. A 0.5 mL sample of the electrolyte after electrolysis was mixed with 0.1 mL of internal standard containg 1.40 mM DMSO solution diluted with D_2O.

It is difficult to accurately compensate applied potentials under high-rate electrolysis due to a significant IR drop and a large Nernstian potential loss associated with pH gradients. In this work, we measured CVs using the current interruption technique[S1,S2] for the IR compensation (Figure S13), and then, the relationship between J_{total} vs. U obtained in these CVs was utilized to evaluate applied potentials for the constant current measurements. The off time was set to 27 msec, and the On/Off ratio was set to 255 in the current interruption. Although we understand the difficulty of the compensation, it has been reported that the current interrupt is one of the ideal compensation methods for high-current CO_2 electrolysis because it can compensate the potential even if solution resistance varies during electrolysis[S3].

Supplementary results

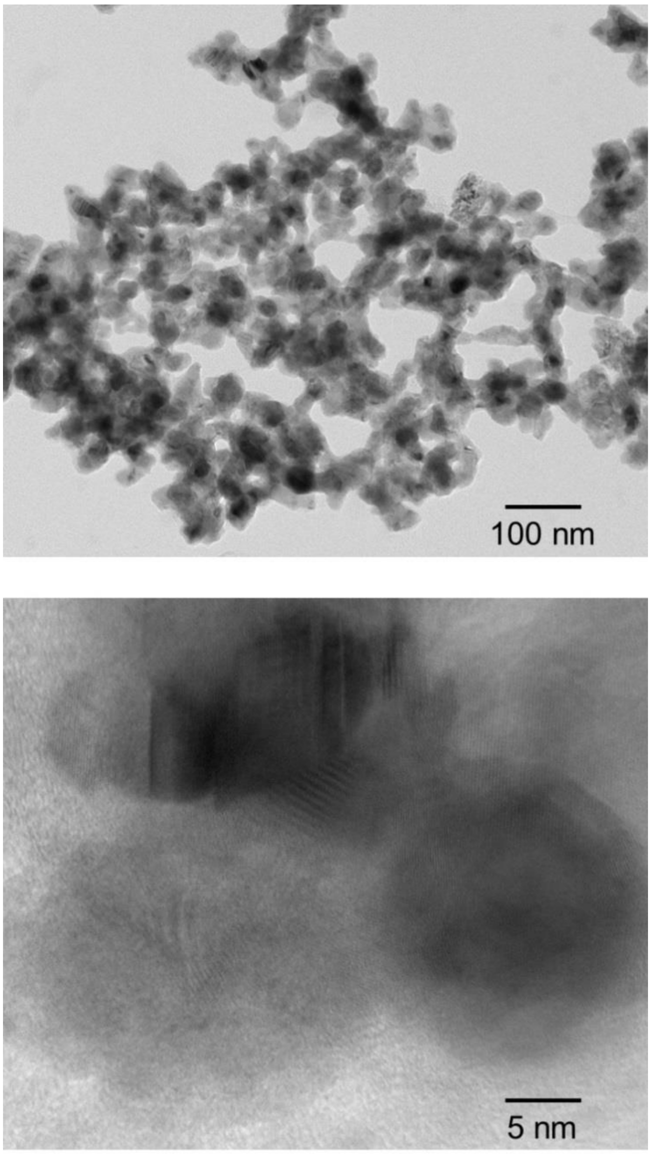

Figure S1 Representative TEM images of the synthesized CuONPs.

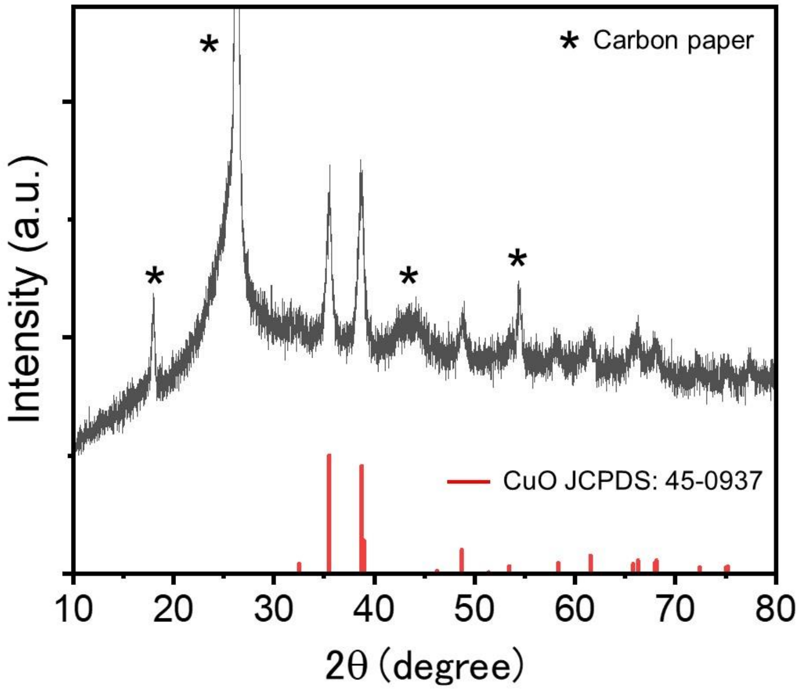

Figure S2 XRD pattern of a CuONPs-1.7/GDE.

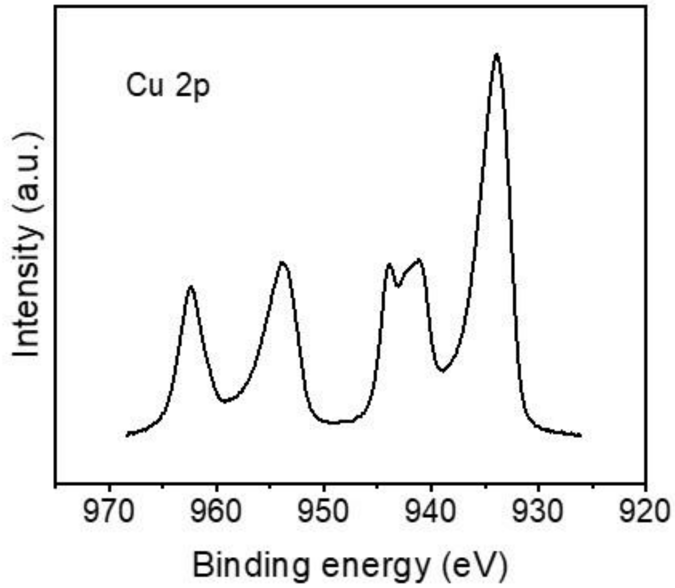

Figure S3 Cu 2p spectrum of CuONPs-1.7/GDE. The main Cu $2p_{3/2}$ peak at 933 eV corresponds to Cu(II) ions. Satellite peaks were observed on the higher binding energy side of the main peaks, which also indicated the presence of Cu(II).

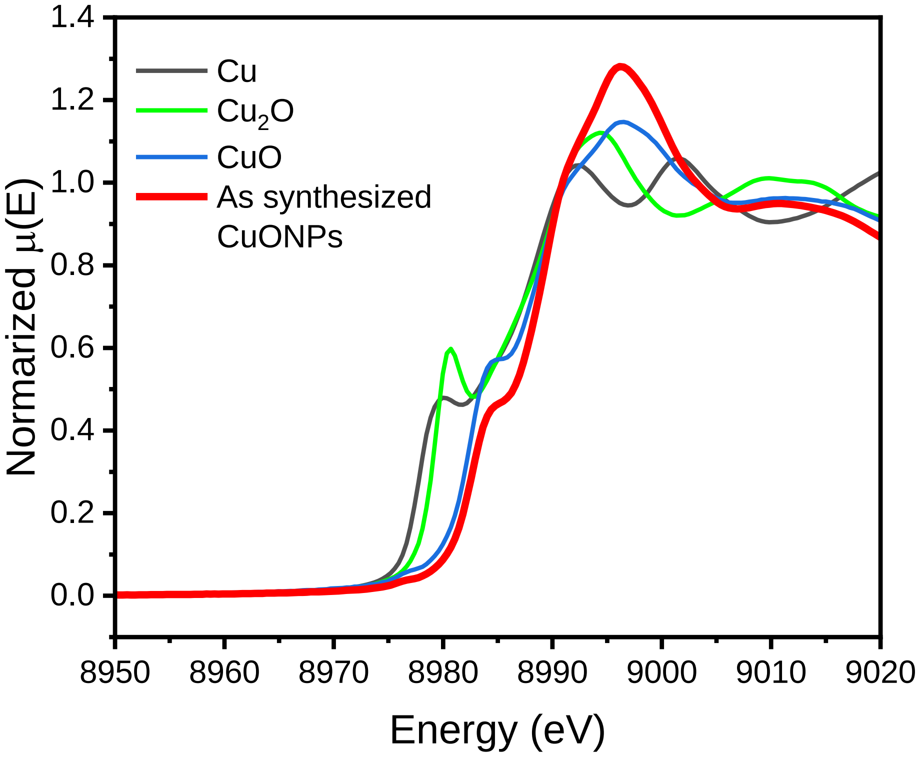

Figure S4 Normalized Cu K-edge XANES spectra of as-synthesized CuONPs.

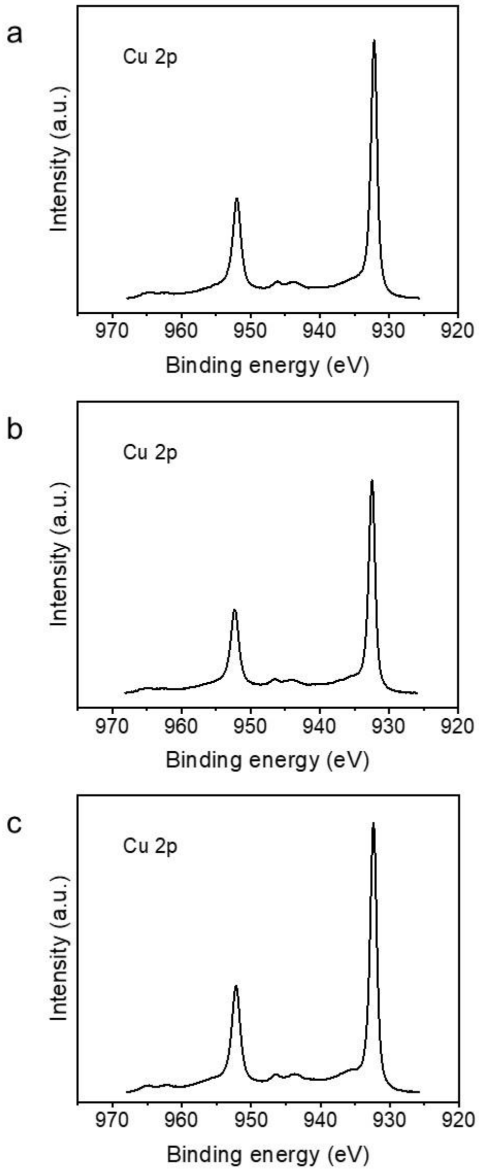

Figure S5 Cu 2p spectra of CuONPs-1.7/GDE after application of (a) J_{total} = 2400 mA/cm^2 for 30 min in 1 M KOH, (b) J_{total} = 2800 mA/cm^2 for 30 min in 1 M KOH, and (c) J_{total} = 2400 mA/cm^2 for 30 min in 1 M KCl. Cu oxidation states were reduced to Cu(I)/Cu(0) during electrolysis, and there was no apparent difference in the surface chemical state of Cu under the different electrolysis conditions (electrolytes or current densities).

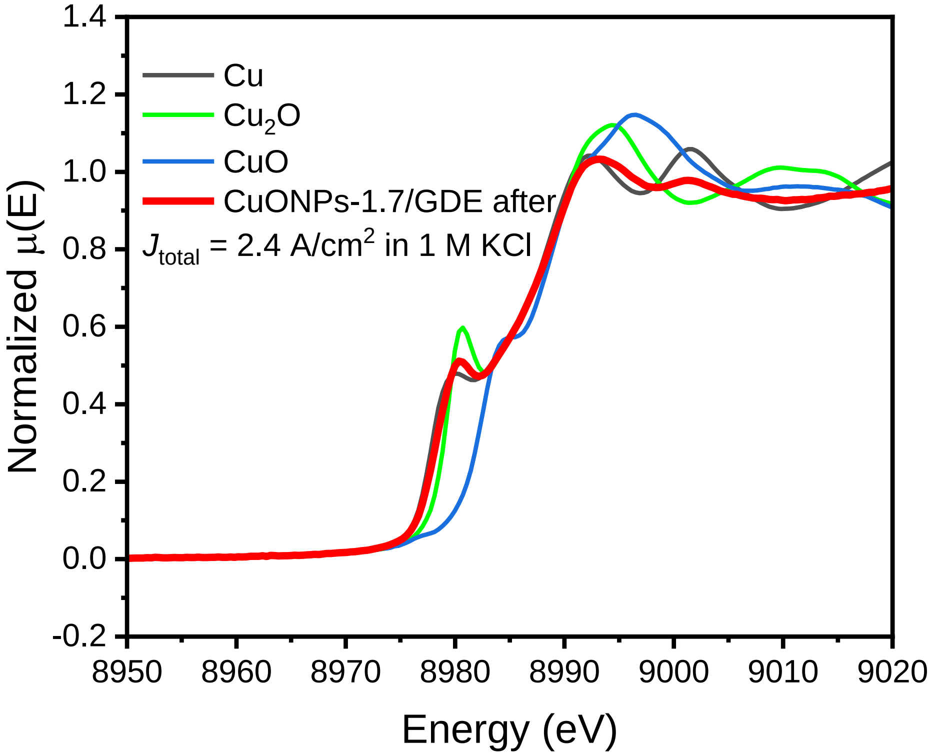

Figure S6 Normalized Cu K-edge XANES spectra of CuONPs-1.7/GDE after applying $J_{total} = 2400$ mA/cm^2 for 30 min in 1 M KCl.

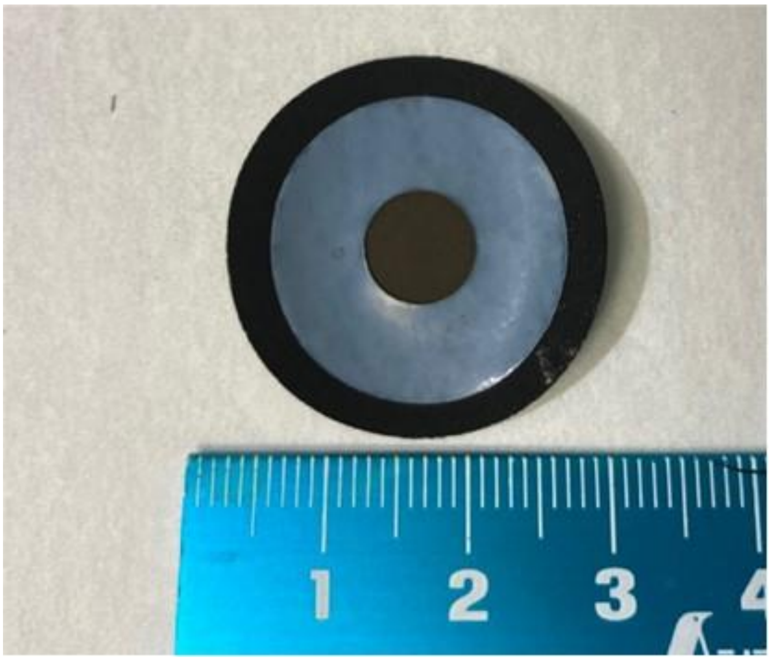

Figure S7 Photograph of the working electrode: CuONPs-deposited on GDE with thermocompressed PTFE (geometric area of the hole is 0.5 cm^2).

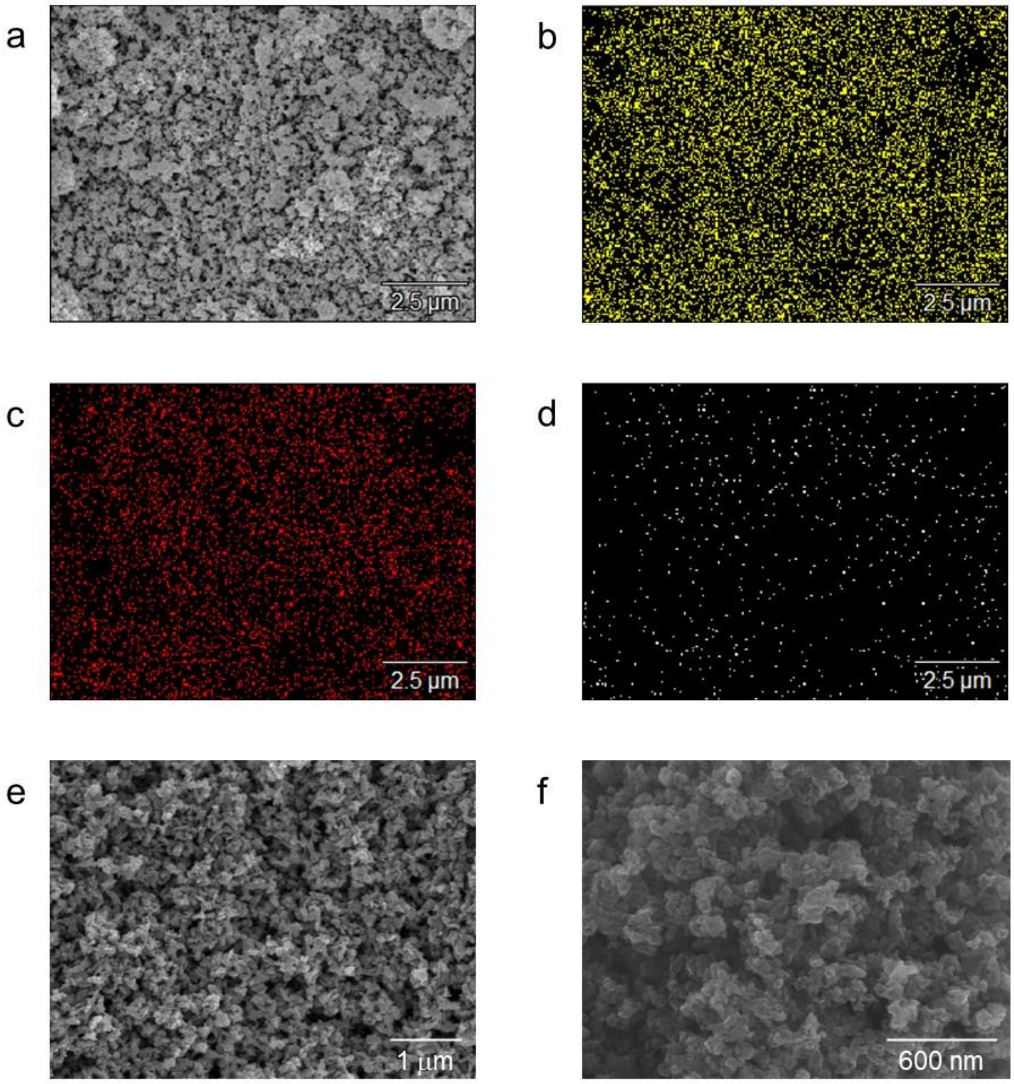

Figure S8 (a)-(f)Top-view SEM images of a CuONPs-1.7/GDE and the corresponding EDX mappings to (a) for (b) Cu, (c) O and (d) C atoms.

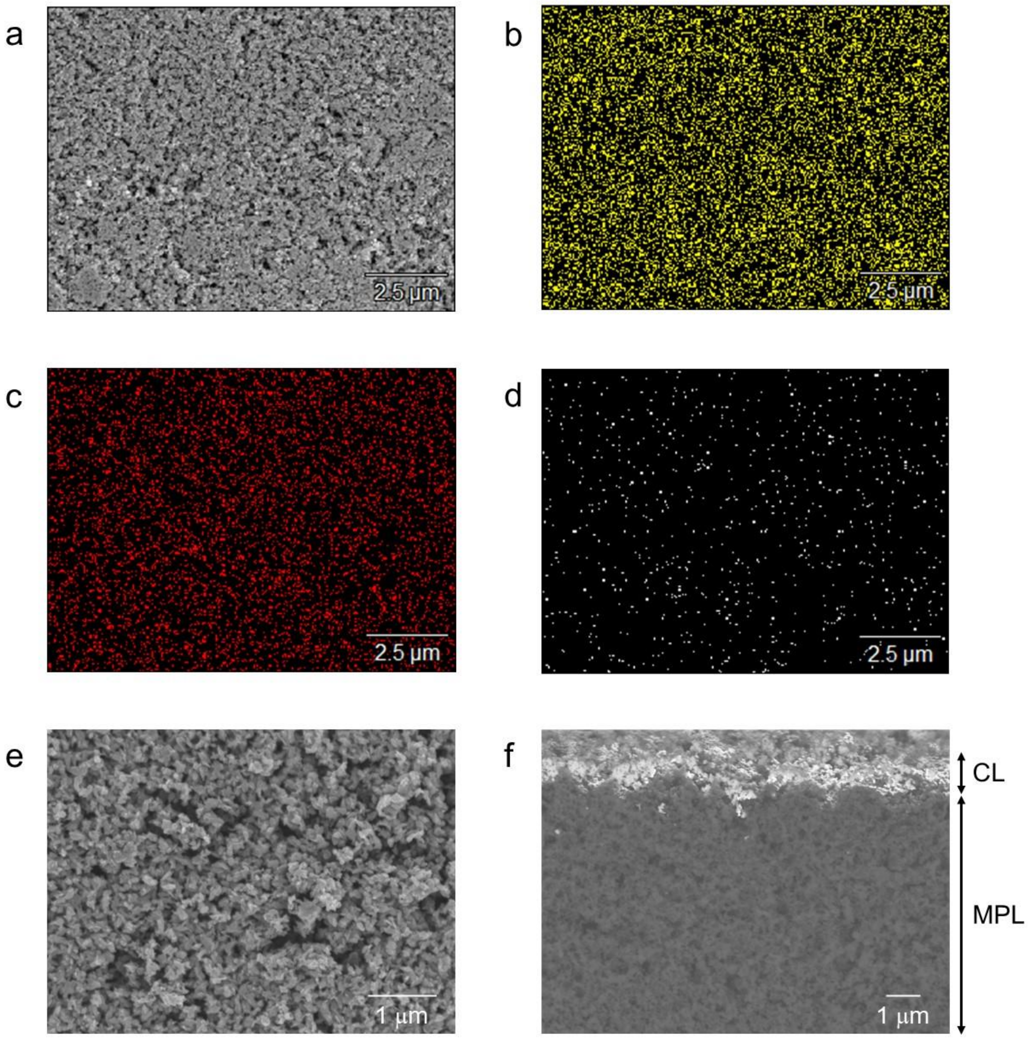

Figure S9 (a-e) Top-view and (f) cross-sectional SEM images of a CuONPs-0.34/GDE and the corresponding EDX mappings to (a) for (b) Cu, (c) O and (d) C atoms.

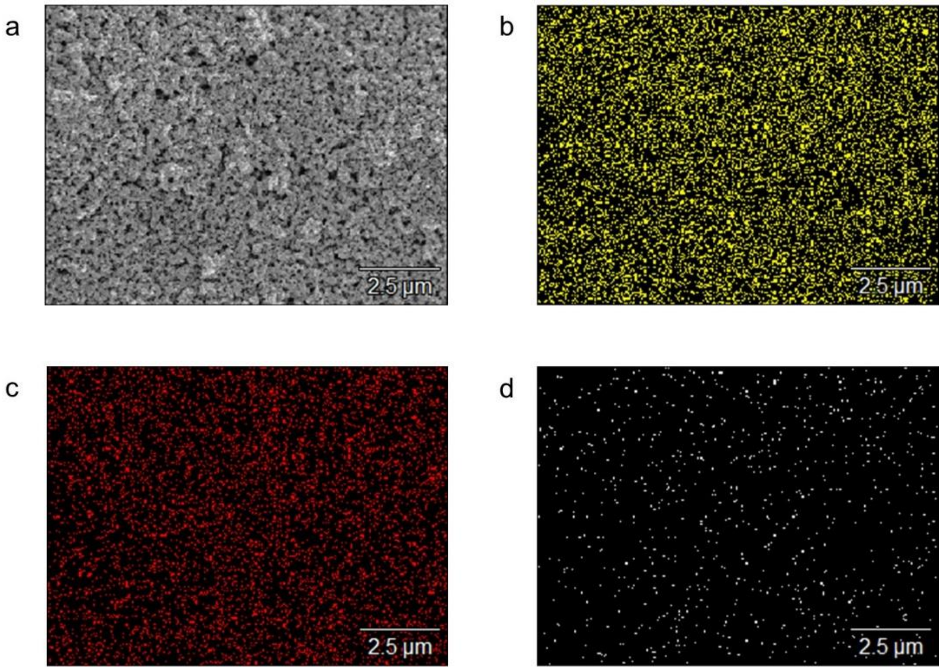

Figure S10 (a) Top-view SEM images of CuONPs-3.1/GDE and the corresponding EDX mappings to (a) for (b) Cu, (c) O and (d) C atoms.

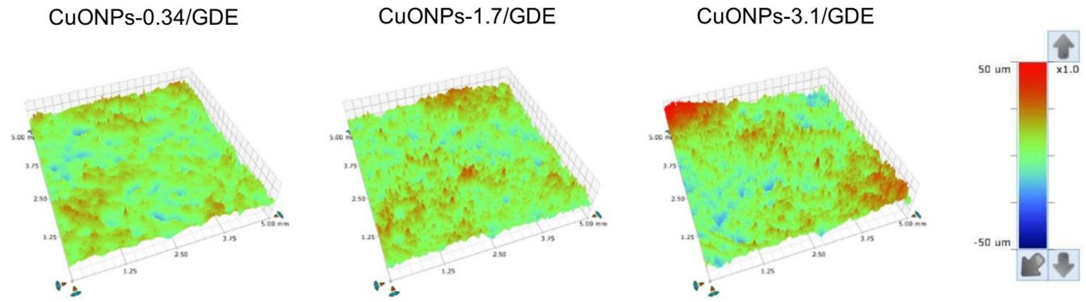

CuONPs-0.34/GDE

CuONPs-1.7/GDE

CuONPs-3.1/GDE

Figure S11 3D Maps of the electrode surface for CuONPs-0.34, 1.7, 3.1/GDE.

Table S1 Roughness factors for CuONPs-0.34, 1.7, 3.1/GDE

	Ra (μm)	Rq (μm)
CuONPs-0.34/GDE	5.697	7.283
CuONPs-1.7/GDE	6.667	8.468
CuONPs-3.1/GDE	8.686	11.32

Ra (arithmetic mean roughness):Average absolute value of deviation from the central plane to the surface on a quantitative surface

Rq (Root mean square roughness): Square root of the mean of the squares of the deviations from the central plane to the surface on a quantitative surface.

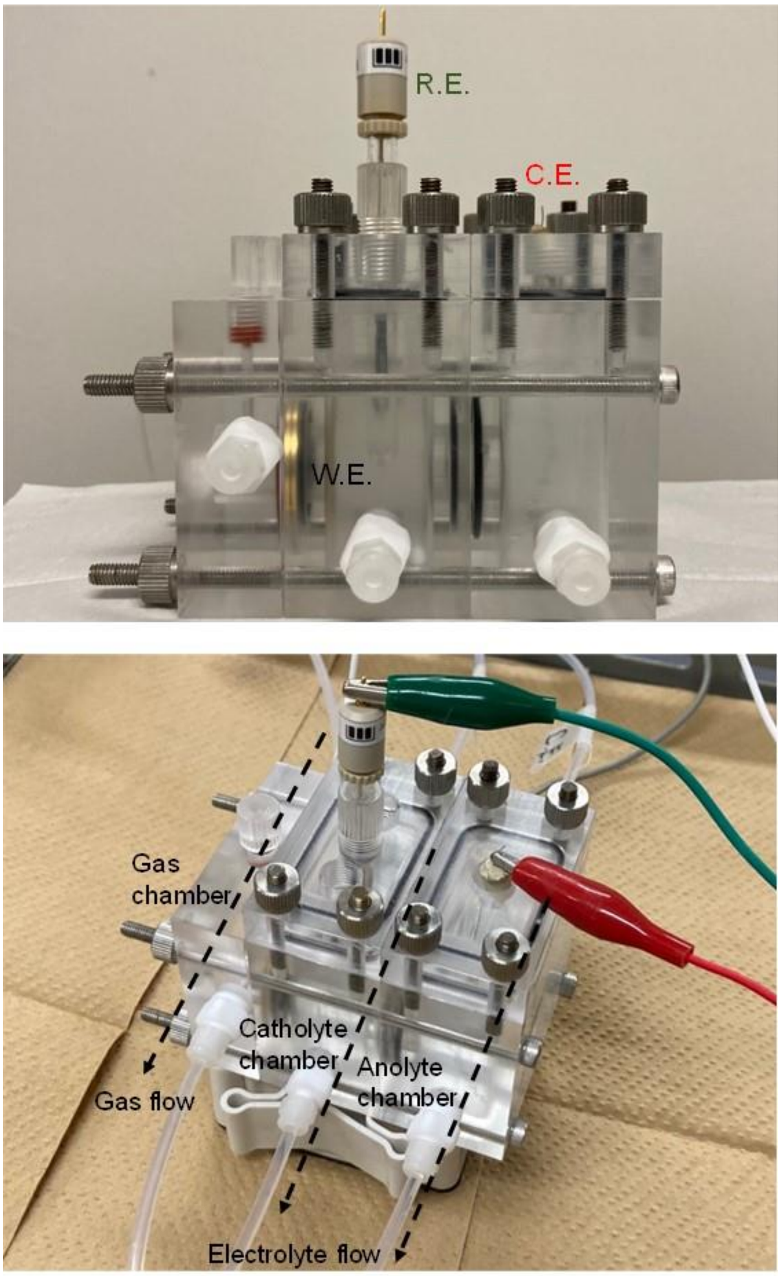

Figure S12 In-house-built three-compartment electrochemical cell for CO_2RR evaluation.

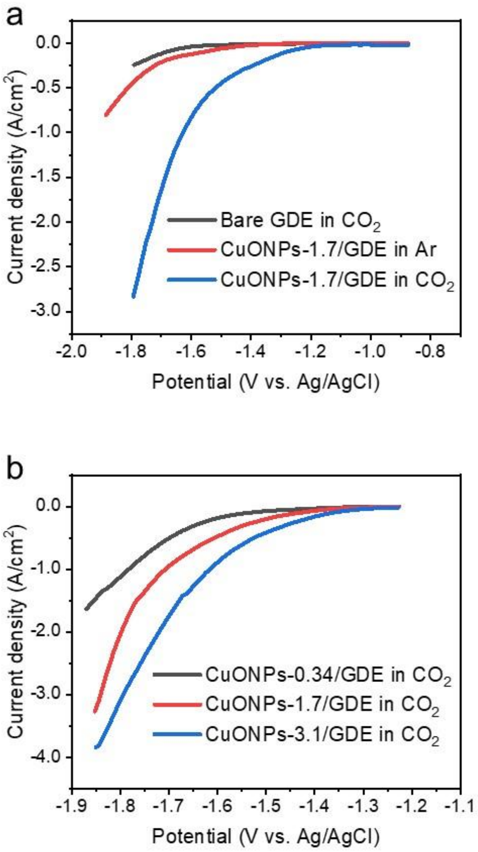

Figure S13 (a) J_{total} vs. U curves for the bare GDE under CO_2, and CuONPs-1.7/GDE under Ar and CO_2 conditions in 1 M KCl electrolyte. (b) J_{total} vs. U curves for the CuONPs-0.34, 1.7, 3.1/GDE under CO_2 conditions in 1 M KOH electrolyte. Scan rate: 50 mV/s

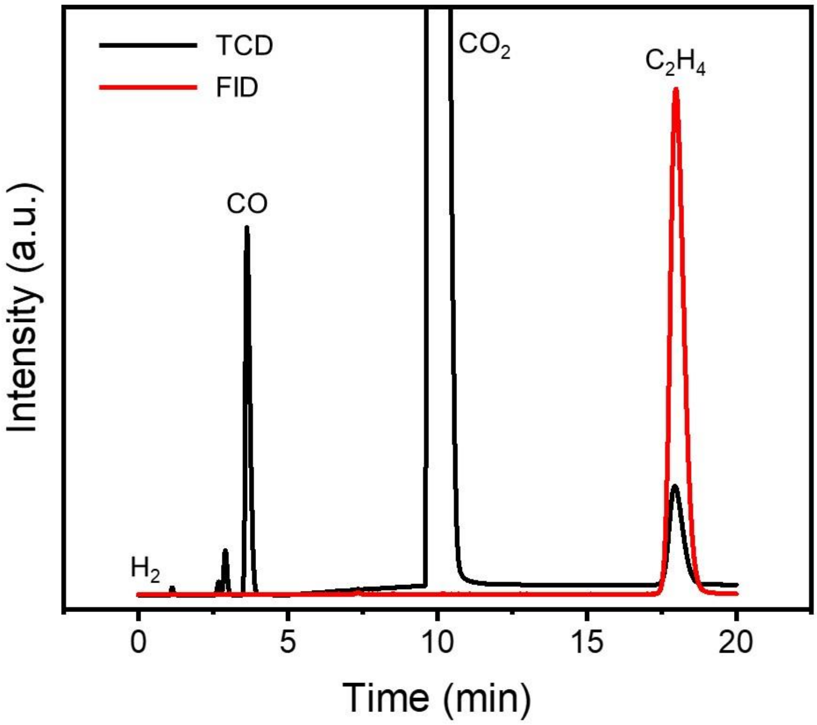

Figure S14 Representative gas chromatography profiles. The gaseous products were analyzed using a gas chromatograph (Shimadzu GC-2030) equipped with a thermal conductivity detector (TCD) and flame ionization detector (FID). CO_2RR conditions: constant current density of $J_{\text{total}} = 1000$ mA/cm^2 for 30 min in 1 M KCl electrolyte.

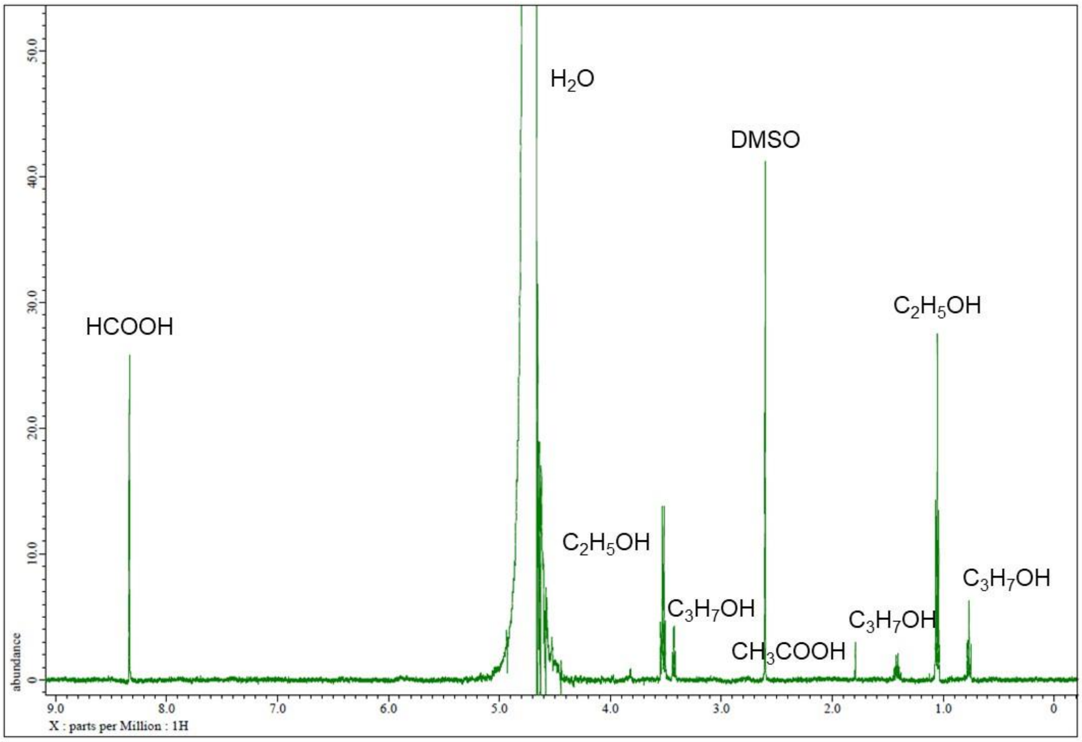

Figure S15 Representative ^{1}H-NMR spectrum. ^{1}H-NMR samples were prepared by mixing 500 μL of the catholyte and 100 μL of DMSO internal standard solution (1.40 mM). ^{1}H-NMR spectra were collected with a water presaturation mode. CO$_2$RR conditions: constant current density of J_{total} = 2000 mA/cm^2 for 30 min in 1 M KCl electrolyte.

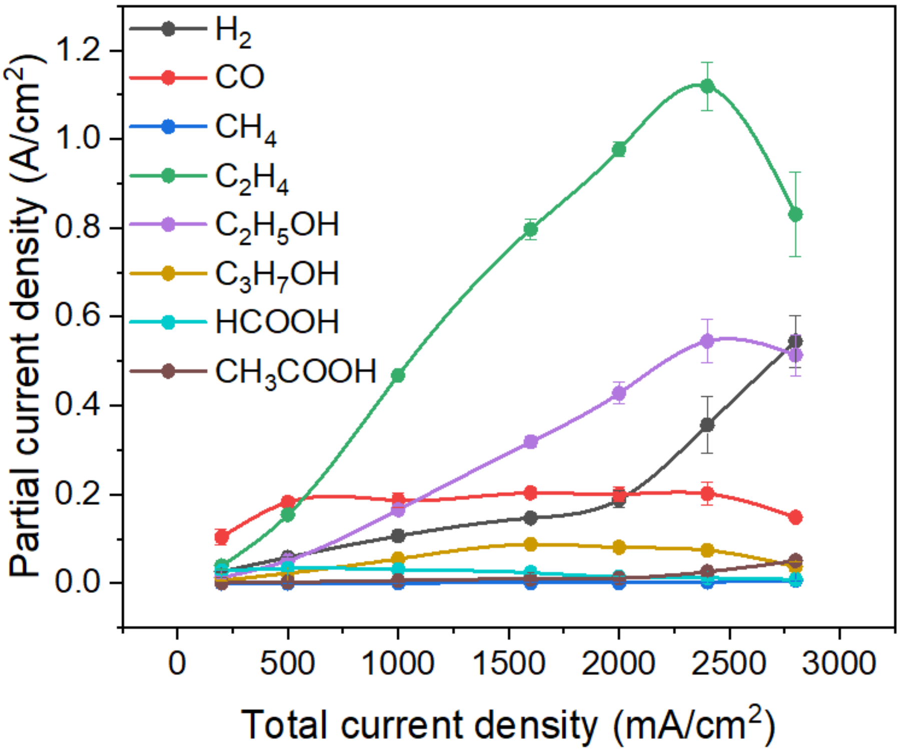

Figure S16 Partial current density of each CO_2RR product on CuONPs-1.7/GDE in 1 M KCl. Reaction time: 30min

Table S2 The comparison of CO_2RR activity in neutral electrolytes. The table shows the highest value of j_{C2+} and FE_{C2+} under those conditions in each reference.

Sample	**Electrolyte**	**FE_{C2+} (%)**	**j_{C2+} (A/cm^2)**	**Ref**
CuONPs-1.7/GDE	1 M KCl	73	1.74	This work
Cu(100)/Cu(111) interface	1 M $KHCO_3$	75	0.22	S4
Cu_2O particle / 30 wt% Nafion	0.1 M $KHCO_3$	62	0.44	S5
Electrodeposited Cu	2 M KCl	67	0.13	S6
Cu derived from Cu	1 M $KHCO_3$	68	0.34	S7
Cu-12	1 M $KHCO_3$	86	0.28	S8
Surface reconstructed Cu	1 M $KHCO_3$	75	0.43	S9

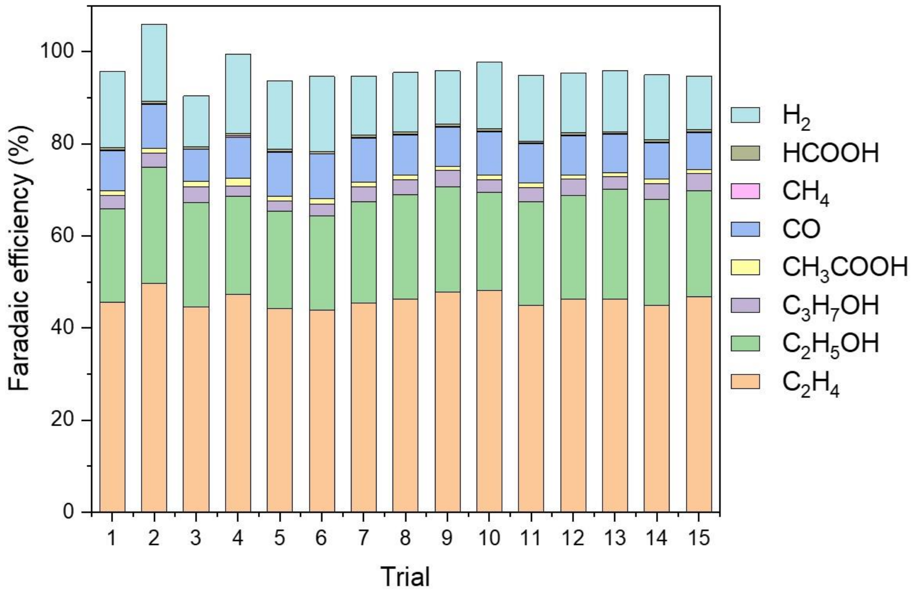

Figure S17 Reproducibility of the CO_2RR results under J_{total} = 2400 mA/cm^2 (j_{C2+} > 1.7 A/cm^2) on CuONPs-1.7/GDE using different batches of electrodes in 1 M KCl. Reaction time: 30 min.

Table S3 Reproducibility of j_{C2+} and faradaic efficiency at J_{total} = 2400 mA/cm^2 on CuONPs-1.7/GDE using different batches of electrodes in 1 M KCl. Reaction time: 30min.

Trial	FE_{C2+}	j_{C2+}	FE_{C2H4}	FE_{C2H5OH}	FE_{C3H7OH}	$FE_{CH3COOH}$	FE_{CO}	FE_{CH4}	FE_{HCOOH}	FE_{H2}
1	69.8	1.67	45.6	20.3	2.9	1.0	8.7	0.2	0.5	16.6
2	79.0	1.90	49.7	25.2	3.0	1.1	9.5	0.1	0.5	16.8
3	71.8	1.72	44.5	22.7	3.4	1.2	7.0	0.1	0.5	11.1
4	72.4	1.74	47.3	21.3	2.2	1.6	9.0	0.2	0.5	17.4
5	68.7	1.65	44.3	21.2	2.1	1.1	9.5	0.2	0.5	14.9
6	68.0	1.63	44.0	20.4	2.5	1.2	9.7	0.2	0.4	16.4
7	71.7	1.72	45.4	21.9	3.4	1.0	9.6	0.1	0.4	13.0
8	73.1	1.76	46.2	22.7	3.4	0.9	8.8	0.1	0.5	12.9
9	75.1	1.80	47.7	23.0	3.6	0.8	8.6	0.1	0.6	11.5
10	73.1	1.75	48.2	21.3	2.7	0.9	9.5	0.2	0.5	14.5
11	71.5	1.72	44.9	22.6	3.1	1.0	8.5	0.1	0.4	14.3
12	73.2	1.76	46.3	22.5	3.5	0.8	8.6	0.1	0.5	13.0
13	73.7	1.77	46.4	23.7	2.7	1.0	8.3	0.2	0.4	13.2
14	72.3	1.74	45.0	23.0	3.4	1.0	8.0	0.2	0.5	14.1
15	74.4	1.79	46.7	23.1	3.7	0.8	8.0	0.1	0.6	11.6
Average	72.5±3.5	1.74±0.08	46.1±1.5	22.3±1.3	3.0±0.5	1.0±0.2	8.8±0.7	0.1±0.04	0.5±0.05	14.1±2.0

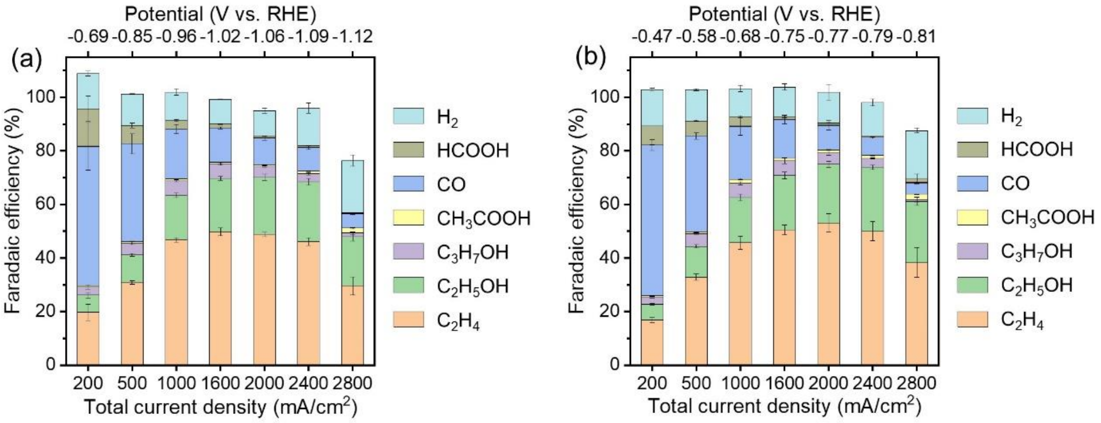

Figure S18 FEs of the CO_2RR products under various applied potentials (V vs. RHE) on CuONPs-1.7/GDE in (a) 1 M KCl (pH: 8) and (b) 1 M KOH (pH: 14).

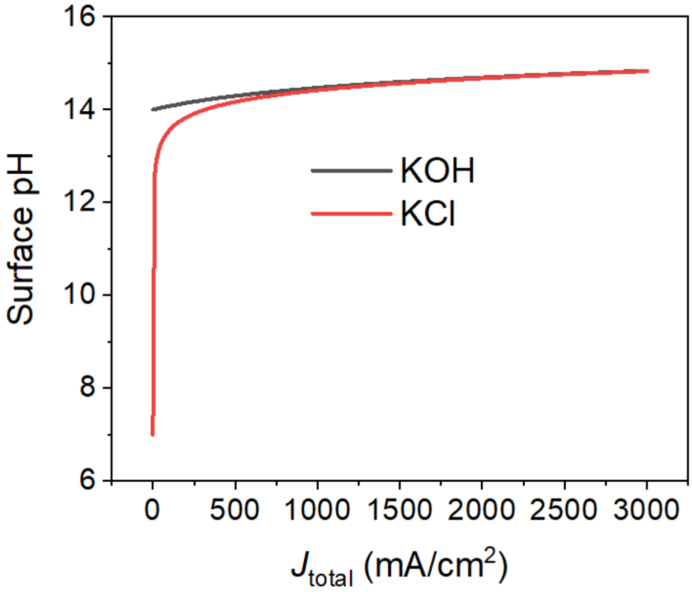

Figure S19 Calculated local pH using a rough reaction-diffusion model.

Table S4 Summary of the reported local pH obtained by theoretical simulations

Electrolyte	Total current density (mA/cm^2)	local pH	References
1 M KCl	200	13.8	this work
1 M KCl	2000	14.7	this work
1 M KOH	200	14.1	this work
1 M KOH	2000	14.7	this work
1 M KCl	200	13.5	S10
1 M KOH	200	14	S10
1 M KOH	200	13.8	S2
1 M KOH	750	15	S11
1 M KCl	100	11.6	S12
1 M KOH	100	12.7	S12
1 M KOH	500	13.2	S12

Table S5 The comparison of CO_2RR activity in alkaline electrolytes. The table shows the highest value of j_{C2+} and FE_{C2+} under those conditions in each reference.

Sample	**Electrolyte**	**FE_{C2+} (%)**	**j_{C2+} (A/cm^2)**	**Ref**
CuONPs-1.7/GDE	1 M KOH	78	1.88	This work
3D CIBH	7 M KOH	78	1.21	S13
F-Cu	0.75 M KOH	80	1.28	S14
Cu-nr/CC3	1 M KOH	76	1.29	S15
N-Cu	1 M KOH	74	0.91	S16
Abrupt Cu interface	3.5 M KOH + 5 M KI	80	0.60	S11
CuAg-wire	1 M KOH	85	0.26	S17
CuS/Cu-V	1 M KOH	53	0.21	S18
CuO-FEP	1 M KOH	77	0.62	S19
Porous Cu	1 M KOH	62	0.40	S20
Cu(100)-rich film	Anion Exchange Membrane	70	0.34	S21
Cu/Fe-N-C s-GDE	0.5 M KOH	90	> 1	S22

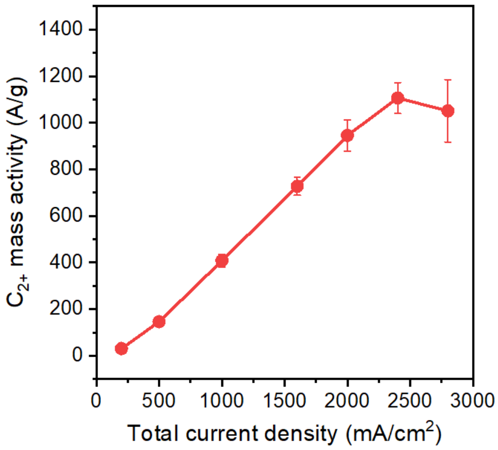

Figure S20 Mass activity for C_{2+} and H_2 production on CuONPs-1.7/GDE in 1 M KOH. Reaction time: 30 min.

Supplementary notes – calculation of TOF (CuONPs-1.7/GDE at J_{total} = 2400 mA/cm^2 in 1 M KOH as an example)

1. Surface area of a CuNP with a diameter of 20.0 nm.

$$4 \times \pi \times (10.0 \times 10^{-9})^2 = 1.26 \times 10^{-15}\ m^2$$

2. Area per copper atom on the surface of CuNPs (assuming the Cu(100) surface, lattice constant: 3.61×10^{-10} m).

$$\frac{(3.61 \times 10^{-10})^2}{2} = 6.52 \times 10^{-20}\ m^2$$

3. Number of Cu atoms on the surface of a CuNP.

$$\frac{1.26 \times 10^{-15}}{6.52 \times 10^{-20}} = 1.93 \times 10^4$$

4. Volume of a CuNP with a diameter of 20 nm.

$$\frac{4 \times \pi \times (10.0 \times 10^{-9})^3}{3} = 4.19 \times 10^{-24} m^3$$

5. Mass of a CuNP with a diameter of 20 nm (assuming that the density is 8.96×10^6 g m^{-3}).

$$4.19 \times 10^{-24} \times 8.96 \times 10^6 = 3.75 \times 10^{-17}\ \text{g}$$

6. Number of CuNPs when the amount of catalyst loading is 1.7 mg/cm^2.

$$\frac{1.7 \times 10^{-3}}{3.75 \times 10^{-17}} = 4.53 \times 10^{13}$$

7. Number of Cu atoms when the amount of catalyst loading is 1.7 mg/cm^2.

$$1.93 \times 10^{4} \times 4.53 \times 10^{13} = 8.74 \times 10^{17}$$

Elementary charge: 1.602×10^{-19}

$$\mathrm{TOF}_{\mathrm{C2H4}} = \frac{jC2H4}{1.602\times10^{-19}\times8.74\times10^{17}\times12} = 0.72$$

$$\mathrm{TOF}_{\mathrm{C2H5OH}} = \frac{jC2H5OH}{1.602\times10^{-19}\times8.74\times10^{17}\times12} = 0.34$$

$$\mathrm{TOF}_{\mathrm{C3H7OH}} = \frac{jC3H7OH}{1.602\times10^{-19}\times8.74\times10^{17}\times12} = 0.03$$

$$\mathrm{TOF}_{\mathrm{CH3COOH}} = \frac{jCH3COOH}{1.602\times10^{-19}\times8.74\times10^{17}\times8} = 0.03$$

$\mathrm{TOF}_{\mathrm{C2+}} = \mathrm{TOF}_{\mathrm{C2H4}} + \mathrm{TOF}_{\mathrm{C2H5OH}} + \mathrm{TOF}_{\mathrm{C3H7OH}} + \mathrm{TOF}_{\mathrm{CH3COOH}} = 1.11\ \mathrm{s}^{-1}$

$\mathrm{TOF}_{\mathrm{C2+}}$ is 1.03 s^{-1} in 1 M KCl on CuONPs-1.7/GDE.

The obtained TOF significantly exceeded the values that have been reported in most of the previous reports. In contrast, several reports exhibited comparable or better TOFs for Cu catalysts[S5, S7, S13, S14], suggesting that our catalysts are not special, but our electrode maximized the potential of Cu catalysts. It must be noted here that we cannot deny a transport limitation affects the TOF values, and thus, these values are just for reference purposes.

Supplementary notes – calculation of energy efficiency (CuONPs-1.7/GDE at $J_{\mathrm{total}} = 2400$ mA/cm^2 in 1 M KCl and 1 M KOH)

$$EE_{full} = \frac{E_{ox} - E_{red}}{E_{cell}} \times FE$$

EE_{full}: full-cell energy efficiency

E_{ox}: thermodynamic potential for water oxidation, i.e. 1.23 V vs. RHE

E_{red}: thermodynamic potential for cathode reaction products

E_{red} = 0 V vs. RHE for H_2

E_{red} = -0.10 V vs. RHE for CO

E_{red} = 0.17 V vs. RHE for CH_4

E_{red} = 0.08 V vs. RHE for C_2H_4

E_{red} = 0.09 V vs. RHE for C_2H_5OH

E_{red} = 0.10 V vs. RHE for C_3H_7OH

E_{red} = -0.12 V vs. RHE for HCOOH

E_{red} = 0.11 V vs. RHE for CH_3COOH

$$EE_{half} = \frac{E_{ox} - E_{red}}{E_{ox} - E_{W-R}} \times FE$$

E_{W-R}: cathode potential (V. vs. RHE)

We also calculated an IR-compensated EE_{half}.

$$EE_{half-IRcomp} = \frac{E_{ox} - E_{red}}{E_{ox} - E_{W-R-IRcomp}} \times FE$$

Table S6 Summary of energy efficiency at $J_{\mathrm{total}} = 2400$ mA/cm^2 in neutral and alkaline electrolytes, respectively.

	Neutral	Alkaline
EE_{full}	6.2 %	7.2 %
EE_{half}	10.5 %	16.7 %
$EE_{\mathrm{half\text{-}IRcomp}}$	48.6 %	56.8 %

Although we really understand that energy efficiency is essential for social implementation, the present study focuses on knowing and elucidating the maximum potential of the CO_2RR electrodes in a half-reaction. Therefore, the gap between the anode and cathode is wide (5 cm), and the anode has not been optimized. Therefore, we are now tackling installing this electrode to membrane electrode assembly cells to achieve a high current density and high energy efficiency simultaneously.

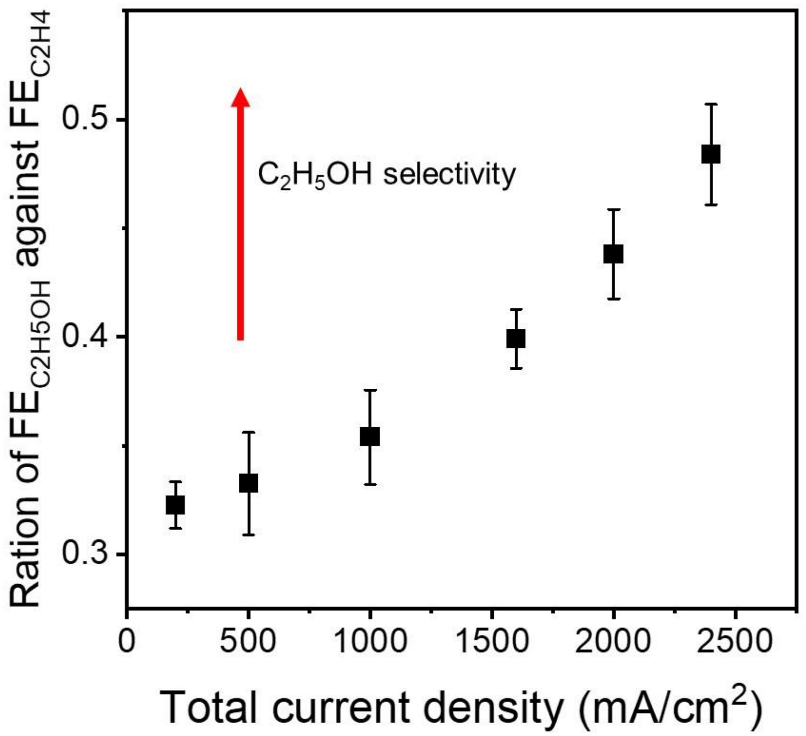

Figure S21 Ratio of FE$_{C2H5OH}$ and FE$_{C2H4}$ against current density over CuONPs-1.7/GDE in 1 M KCl.

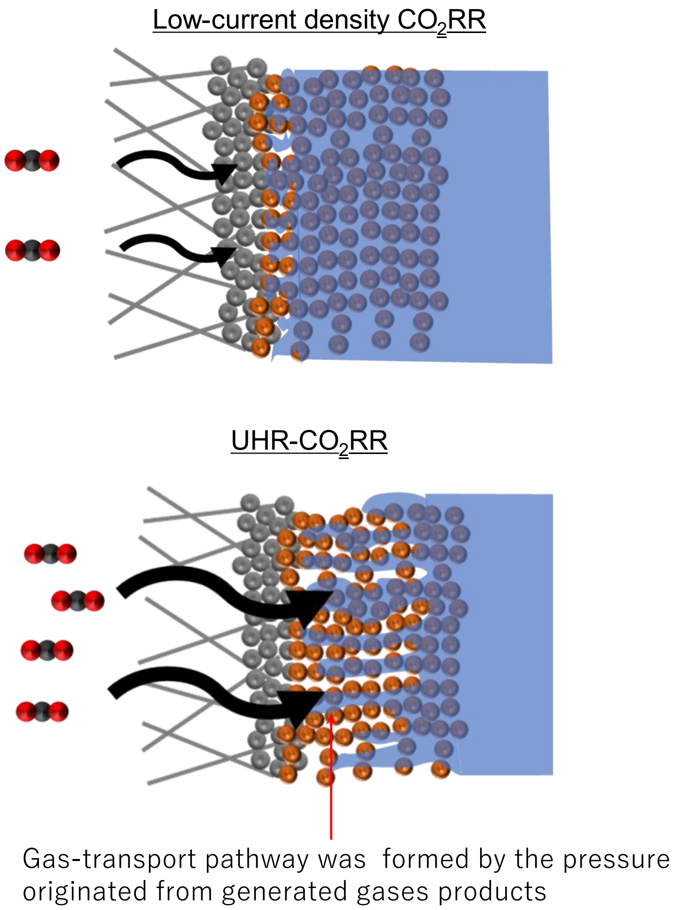

Gas-transport pathway was formed by the pressure originated from generated gases products

Figure S22 A schematic illustration of *in situ* formation of the gas-transport pathway.

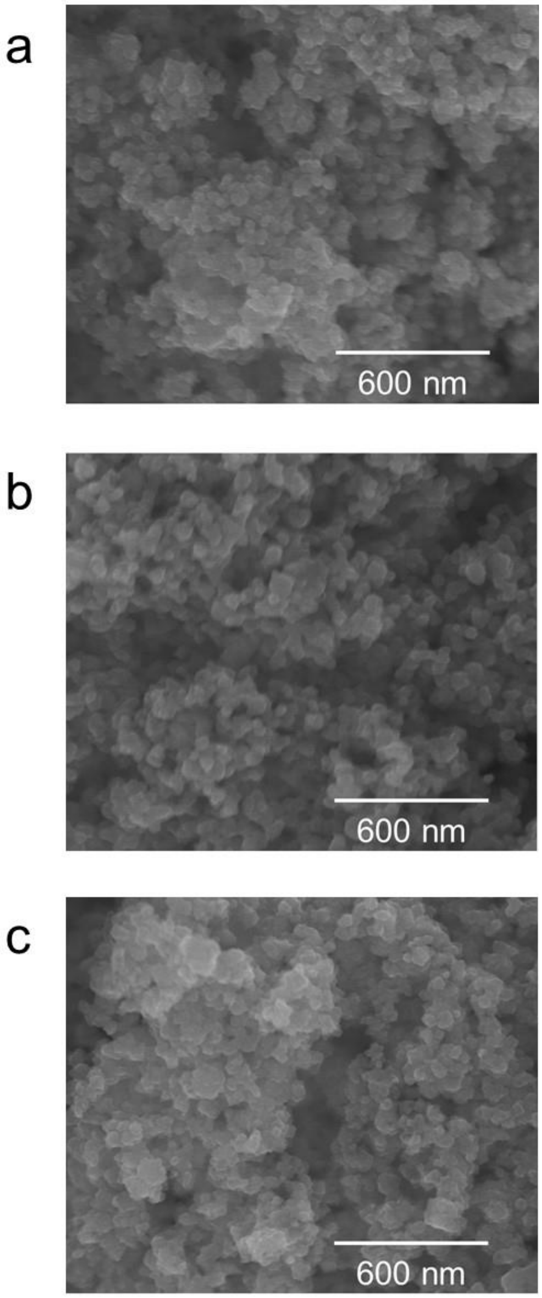

Figure S23 Top-view SEM images of CuONPs-1.7/GDE after application of J_{total} = (a) 2400 mA/cm^2 in 1 M KCl, (b) 2800 mA/cm^2 in 1 M KCl, and (c) 2400 mA/cm^2 in 1 M KOH for 30 min.

The surface morphology did not significantly change during CO_2RR. These SEM images were acquired after rinsing the surface and drying under vacuum conditions.

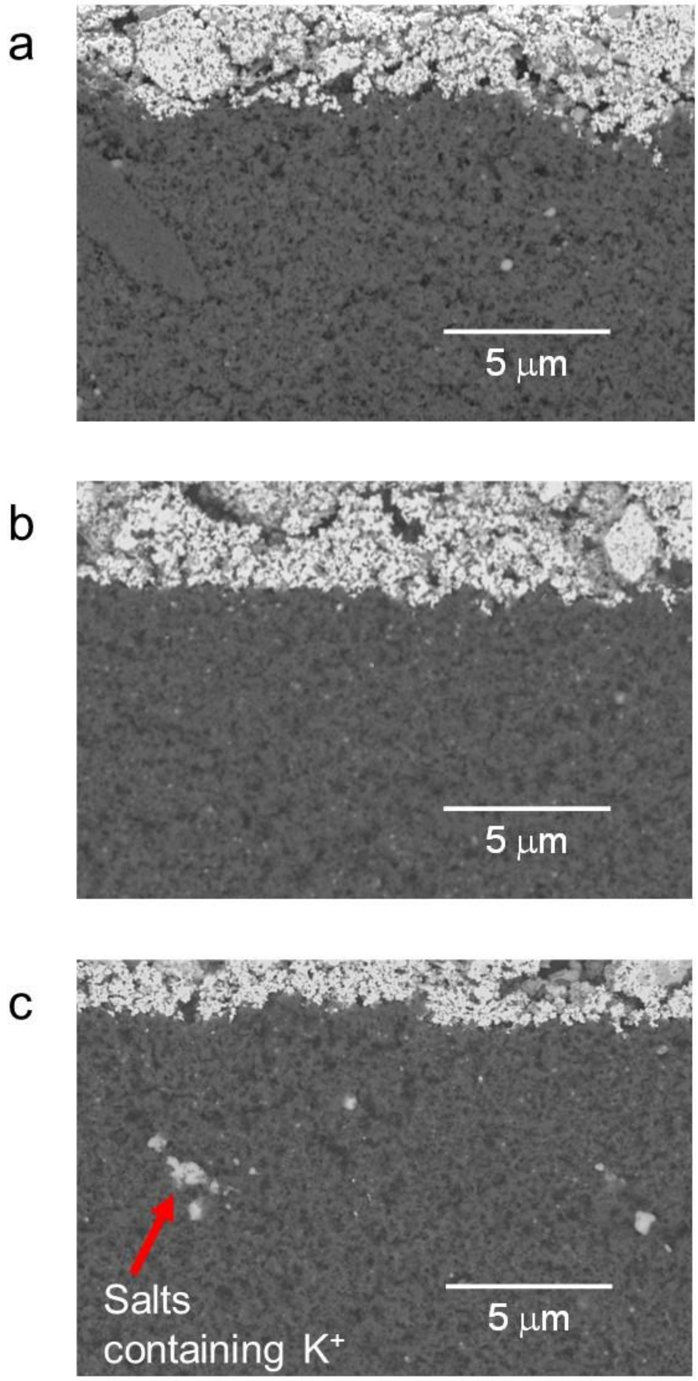

Figure S24 Accumulation of salts containing K$^+$ in the MPL of CuONPs-1.7/GDE after application of J_{total} = (a) 1000 mA/cm^2, (b) 2000 mA/cm^2, and (c) 2800 mA/cm^2 for 30 min under CO$_2$RR conditions in 1 M KCl. These SEM images were acquired after freeze-drying the electrodes.

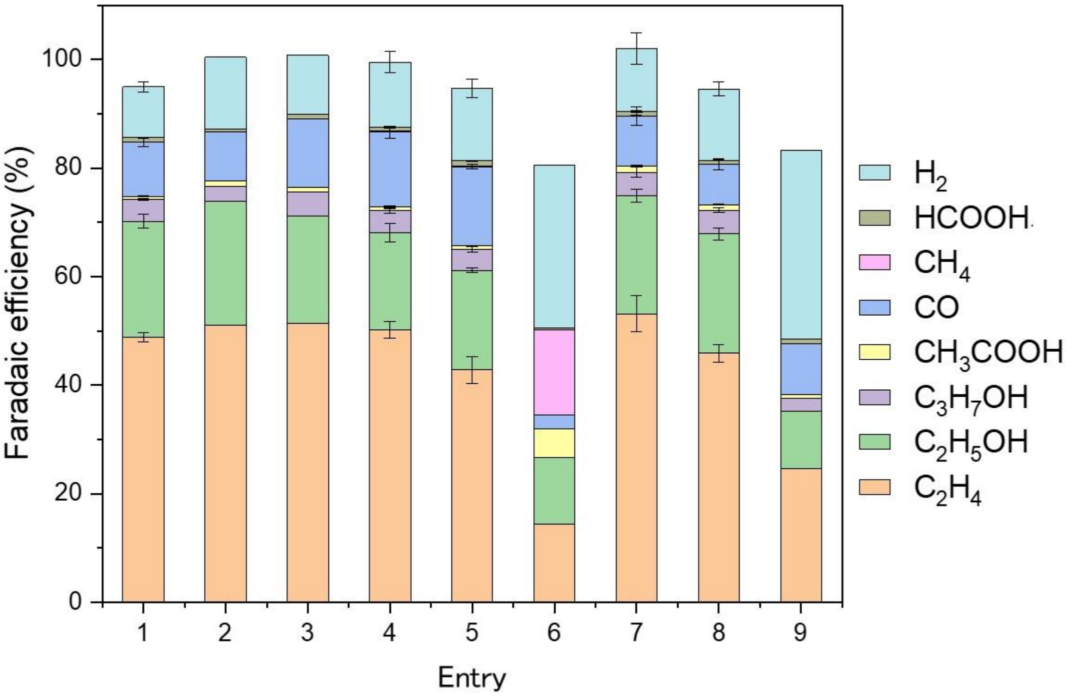

Entry	GDL	Catalyst	Electrolyte
1	34BC	CuONPs-1.7/GDE	1 M KCl
2	MFK-A	CuONPs-1.7/GDE	1 M KCl
3	GDS2130	CuONPs-1.7/GDE	1 M KCl
4	34BC	CuO 50 nm (sigma)-1.7/GDE	1 M KCl
5	34BC	CuONPs-1.7/GDE	1 M KHCO3
6	34BC	CuONPs-0.34/GDE	1 M KOH
7	34BC	CuONPs-1.7/GDE	1 M KOH
8	34BC	CuONPs-3.1/GDE	1 M KOH
9	34BC	CuONPs-10/GDE	1 M KOH

Figure S25 and Table S7 Faradaic efficiency of CO_2RR products under J_{total} = 2000 mA/cm^2 when changing GDEs, catalysts, the thickness of CL, and electrolytes.

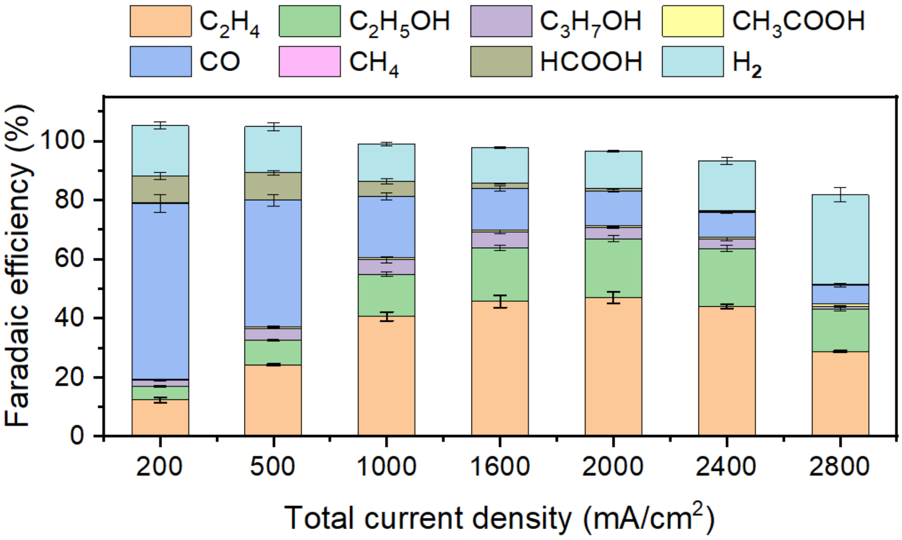

Figure S26 FEs of the CO_2RR products under different applied potentials over CuONPs-3.1/GDE in 1 M KCl under constant current measurements. Reaction time: 30 min.

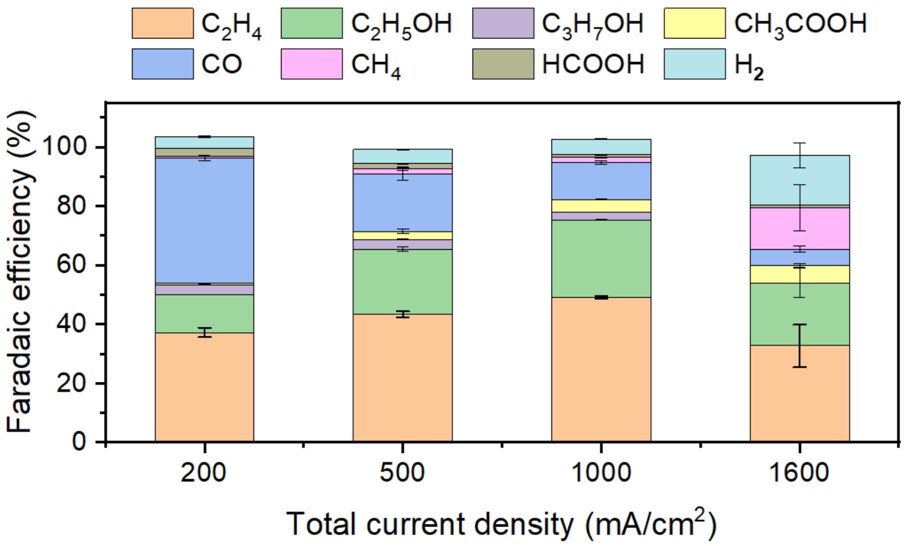

Figure S27 FEs of the CO_2RR products under different applied potentials over CuONPs-0.34/GDE in 1 M KCl under constant current measurements. Reaction time: 30 min.

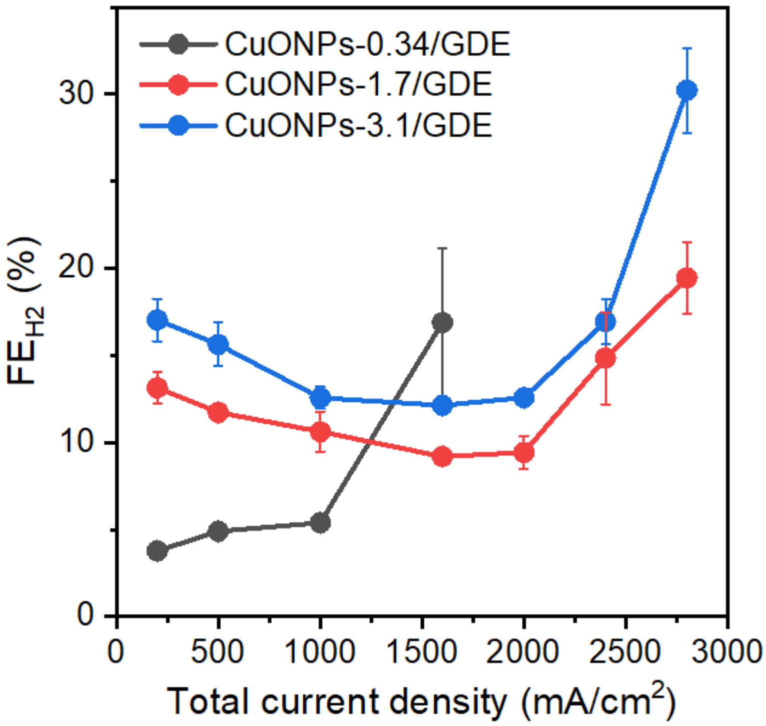

Figure S28 FE_{H2} against J_{total} for various amounts of Cu loading (CuONPs-0.34, -1.7 and -3.1/GDE) in 1 M KCl. Reaction time: 30 min.

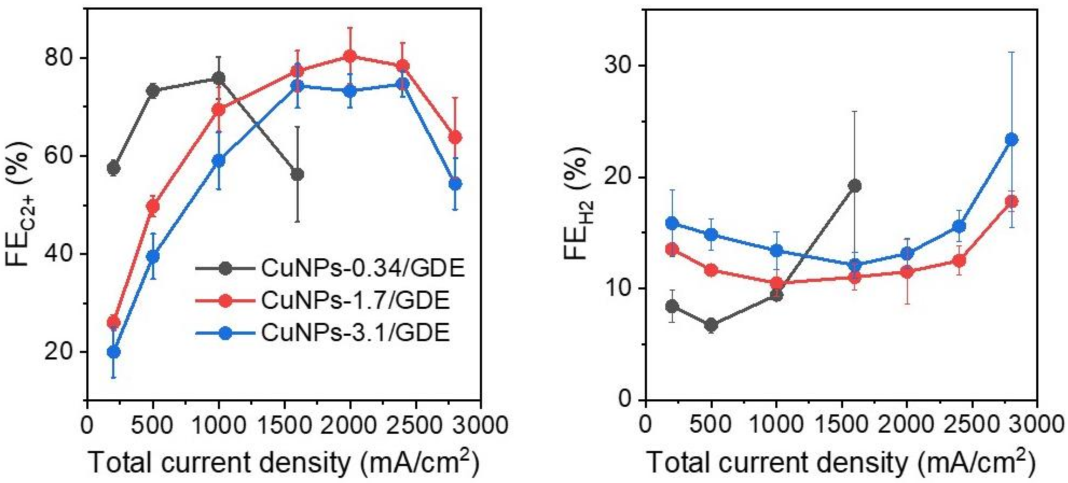

Figure S29 (a)FE$_{C2+}$ and (b)FE$_{H2}$ against J_{total} for various amounts of Cu loading (CuONPs-0.34, -1.7 and -3.1/GDE) in 1 M KOH. Reaction time: 30 min.

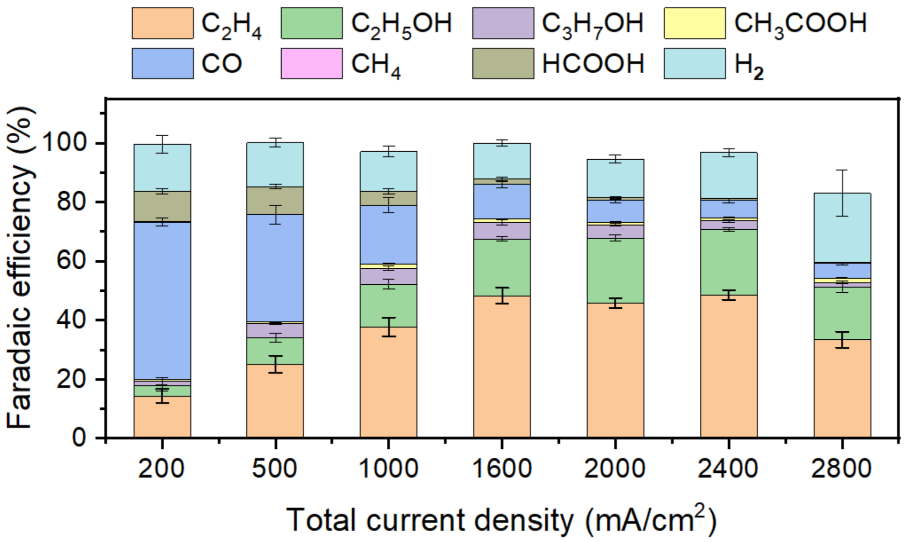

Figure S30 FEs of the CO_2RR products under different applied potentials over CuONPs-3.1/GDE in 1 M KOH under constant current measurements. Reaction time: 30 min.

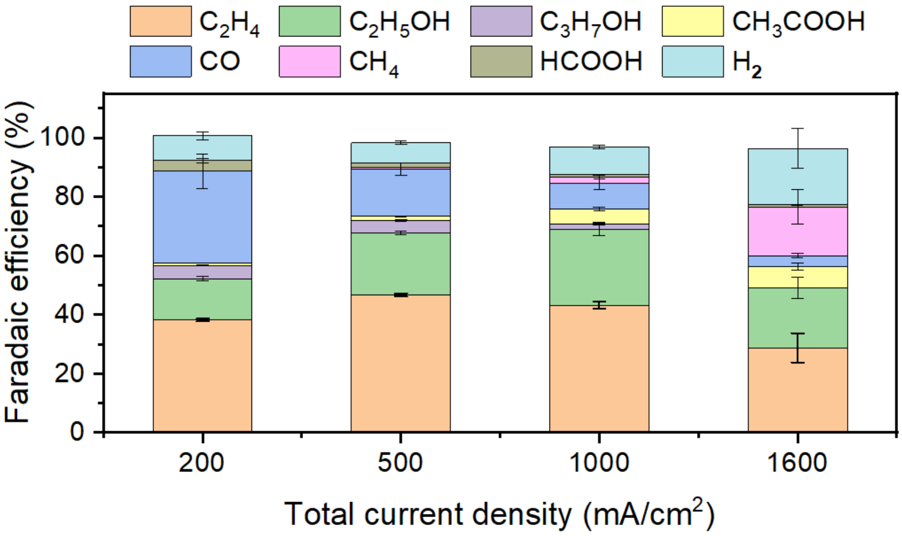

Figure S31 FEs of the CO_2RR products under different applied potentials over CuONPs-0.34/GDE in 1 M KOH under constant current measurements. Reaction time: 30 min.

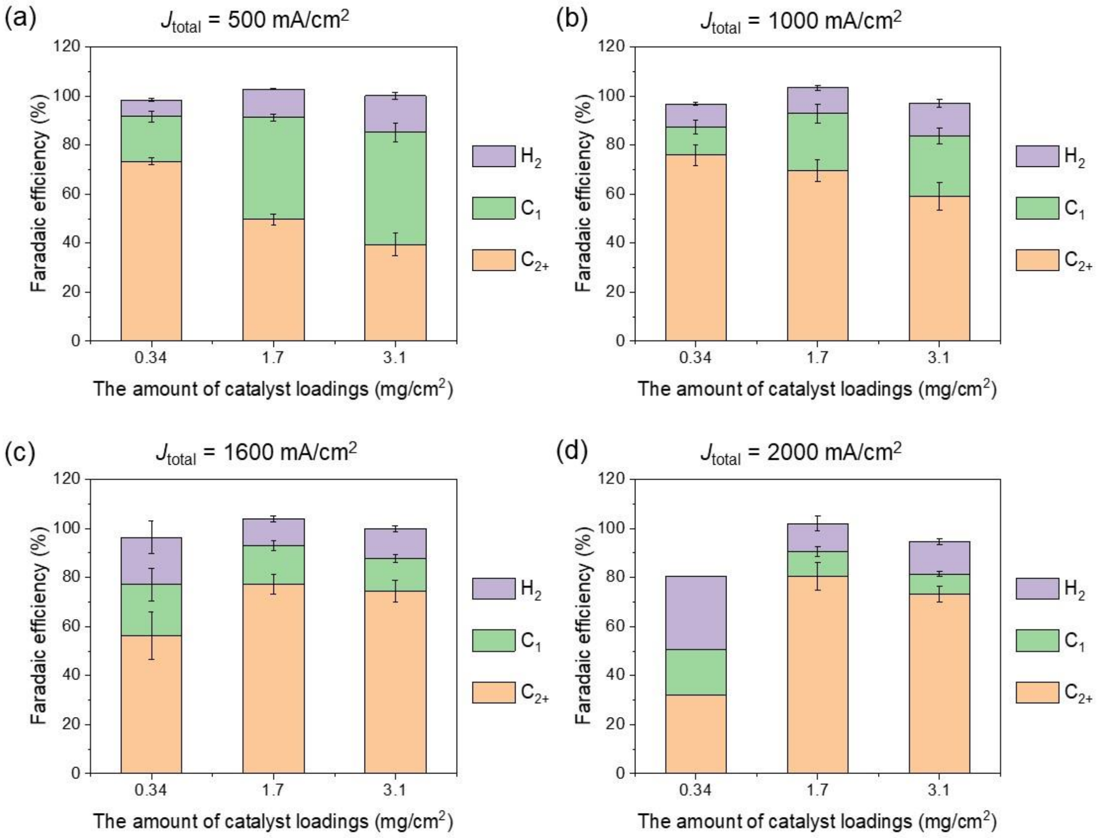

Figure S32 FE$_{C2+}$. FE$_{C1}$, and FE$_{H2}$ depending on the amount of catalyst loadings at J_{total} = (a) 500 mA/cm^2, (b) 1000 mA/cm^2, (c) 1600 mA/cm^2 and (d) 2000 mA/cm^2 in 1 M KOH. Reaction time: 30min.

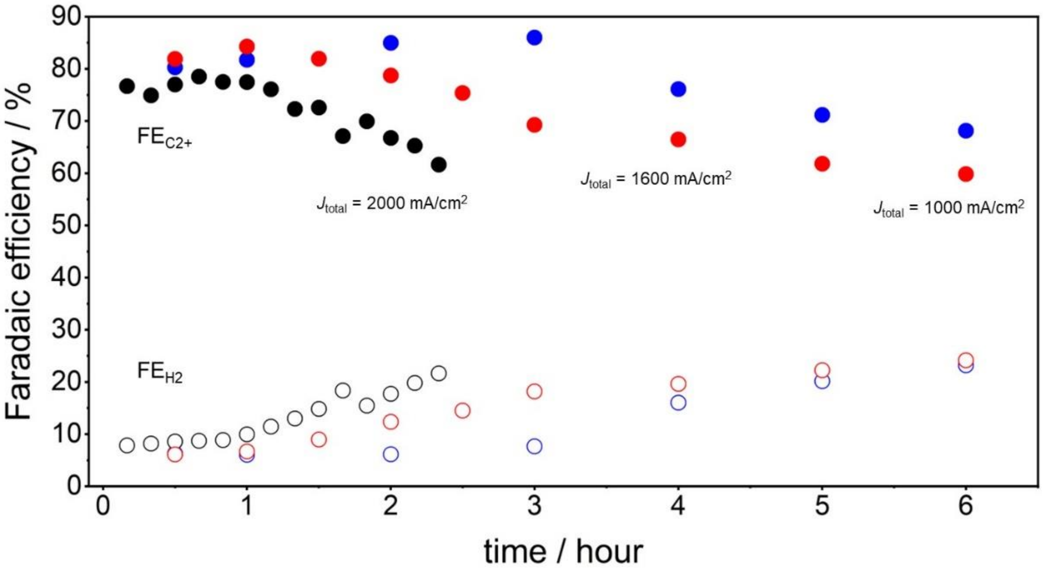

Figure S33 Stability tests with respect to the total current density. The filled and blank points show FE_{C2+} and FE_{H2}, respectively, over CuONPs-1.0/GDE in 1 M KCl under J_{total} = 2000 mA/cm^2 (black), 1600 mA/cm^2 (red) and 1000 mA/cm^2 (blue).

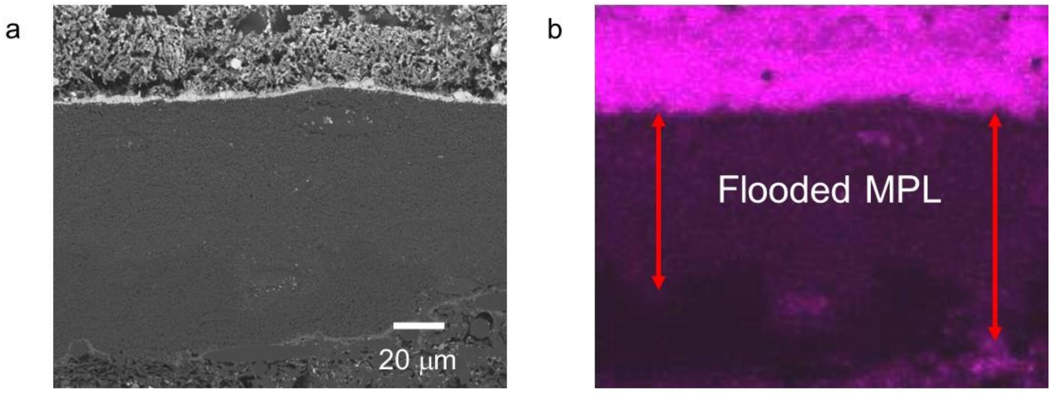

Figure S34 (a) A cross-sectional SEM image of CuONPs-1.0/GDE and (b) K^+ distribution (purple) obtained by EDX after application of J_{total} = 1600 mA/cm^2 for 6 h under CO_2RR conditions in 1 M KCl.

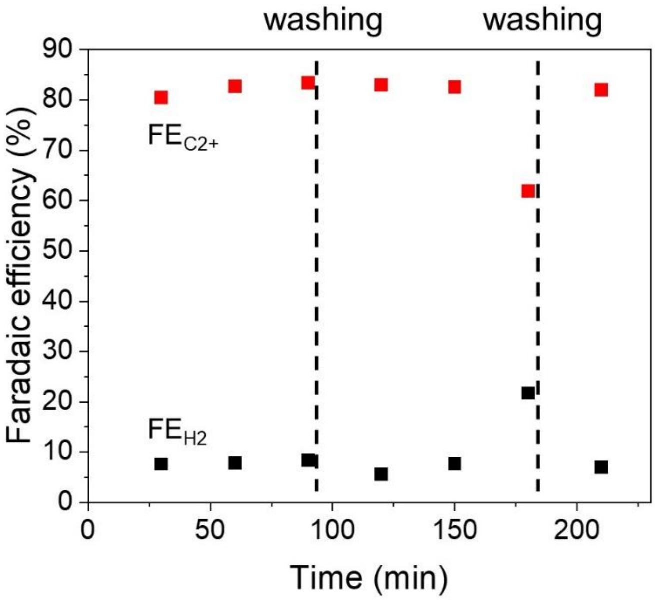

Figure S35 Recycling test on CuONPs-1.0/GDE in 1 M KCl under J_{total} = 1600 mA/cm^2. FE$_{C2+}$ value was recovered by washing the electrode with pure water indicating that the decrease in FE$_{C2+}$ after prolonged operation was due to the salt precipitation induced by flooded MPL.

References

S1. D. Kopljar, N. Wagner and E. Klemm, *Chem. Eng. Technol.*, 2016, **39**, 2042-2050.

S2. K. Liu, W. A. Smith and T. Burdyny, *ACS Energy Lett.*, 2019, **4**, 639-643.

S3. Heenan, A. R., Hamonnet, J. and Marshall, A. T, *ACS Energy Lett.*, 2022, **7**, 2357–2361.

S4. Z. Z. Wu, X. L. Zhang, Z. Z. Niu, F. Y. Gao, P. P. Yang, L. P. Chi, L. Shi, W. S. Wei, R. Liu, Z. Chen, S. Hu, X. Zheng and M. R. Gao, *J. Am. Chem. Soc.*, 2022, **144**, 259-269.

S5. T. Möller, T. Ngo Thanh, X. Wang, W. Ju, Z. Jovanov and P. Strasser, *Energy Environ. Sci.*, 2021, **14**, 5995-6006.

S6. X. Zhang, J. Li, Y. Y. Li, Y. Jung, Y. Kuang, G. Zhu, Y. Liang and H. Dai, *J. Am. Chem. Soc.*, 2021, **143**, 3245-3255.

S7. Y. C. Tan, K. B. Lee, H. Song and J. Oh, *Joule*, 2020, **4**, 1104-1120.

S8. F. Li, A. Thevenon, A. Rosas-Hernández, Z. Wang, Y. Li, C. M. Gabardo, A. Ozden, C. T. Dinh, J. Li, Y. Wang, J. P. Edwards, Y. Xu, C. McCallum, L. Tao, Z. Q. Liang, M. Luo, X. Wang, H. Li, C. P. O'Brien, C. S. Tan, D. H. Nam, R. Quintero-Bermudez, T. T. Zhuang, Y. C. Li, Z. Han, R. D. Britt, D. Sinton, T. Agapie, J. C. Peters and E. H. Sargent, *Nature*, 2020, **577**, 509-513.

S9. M. G. Kibria, C. T. Dinh, A. Seifitokaldani, P. De Luna, T. Burdyny, R. Quintero-Bermudez, M. B. Ross, O. S. Bushuyev, F. P. García de Arquer, P. Yang, D. Sinton and E. H. Sargent, *Adv. Mater.*, 2018, **30**, 1804867.

S10. Burdyny, T. and Smith, W. A., *Energy Environ. Sci.*, 2019, **12**, 1442–1453.

S11. C. T. Dinh, T. Burdyny, G. Kibria, A. Seifitokaldani, C. M. Gabardo, F. Pelayo García De Arquer, A. Kiani, J. P. Edwards, P. De Luna, O. S. Bushuyev, C. Zou, R. Quintero-Bermudez, Y. Pang, D. Sinton and E. H. Sargent, *Science*, 2018, **360**, 783-787.

S12. H. Guzmán, F. Zammillo, D. Roldán, C. Galletti, N. Russo, and S. Hernández., *Catalysts,* 2021, **11**, 482.

S13. F. P. García de Arquer, C. T. Dinh, A. Ozden, J. Wicks, C. McCallum, A. R. Kirmani, D. H. Nam, C. Gabardo, A. Seifitokaldani, X. Wang, Y. C. Li, F. Li, J. Edwards, L. J. Richter, S. J. Thorpe, D. Sinton and E. H. Sargent, *Science*, 2020, **367**, 661-666.

S14. W. Ma, S. Xie, T. Liu, Q. Fan, J. Ye, F. Sun, Z. Jiang, Q. Zhang, J. Cheng and Y. Wang, *Nat. Catal.*, 2020, **3**, 478-487.

S15. C. Chen, X. Yan, Y. Wu, S. Liu, X. Zhang, X. Sun, Q. Zhu, H. Wu and B. Han, *Angew. Chem. Int. Ed.*, 2022, **61**, e2022026.

S16. M. Zheng, P. Wang, X. Zhi, K. Yang, Y. Jiao, J. Duan, Y. Zheng and S. Qiao, *J. Am. Chem. Soc.*, 2022, **144**, 14936-14944.

S17. T. T. H. Hoang, S. Verma, S. Ma, T. T. Fister, J. Timoshenko, A. I. Frenkel, P. J. A. Kenis and A. A. Gewirth, *J. Am. Chem. Soc.*, 2018, **140**, 5791-5797.

S18. T. T. Zhuang, Z. Q. Liang, A. Seifitokaldani, Y. Li, P. De Luna, T. Burdyny, F. Che, F. Meng, Y. Min, R. Quintero-Bermudez, C. T. Dinh, Y. Pang, M. Zhong, B. Zhang, J. Li, P. N. Chen, X. L. Zheng, H. Liang,

W. N. Ge, B. J. Ye, D. Sinton, S. H. Yu and E. H. Sargent, *Nat. Catal.*, 2018, **1**, 421-428.

S19. T. H. M. Pham, J. Zhang, M. Li, T. H. Shen, Y. Ko, V. Tileli, W. Luo and A. Züttel, *Adv. Energy Mater.*, 2022, **12**, 2103663.

S20. J. J. Lv, M. Jouny, W. Luc, W. Zhu, J. J. Zhu and F. Jiao, *Adv. Mater.*, 2018, **30**, 1803111.

S21. G. Zhang, Z. J. Zhao, D. Cheng, H. Li, J. Yu, Q. Wang, H. Gao, J. Guo, H. Wang, G. A. Ozin, T. Wang and J. Gong, *Nat. Commun.*, 2021, **12**, 5745.

S22. T. Zhang, J. C. Bui, Z. Li, A. T. Bell, A. Z. Weber and J. Wu, *Nat. Catal.*, 2022, **5**, 202-211.